Fatigue Life Estimation of Local Sharp-grooved Circular Tubes with Different Diameter-to-thickness Ratios under Cyclic Bending

Kuo-Long Lee[1], and Wen-Fung Pan[2]

[1] Department of Innovative Design and Entrepreneurship Management, Far East University, Tainan 744, Taiwan

[2] Department of engineering Science, National Cheng Kung University, Tainan 701, Taiwan

Abstract

In this paper, the fatigue life estimation of local sharp-grooved 6061-T6 aluminum alloy tubes with different diameter-to-thickness ratios under cyclic bending are studied. Different diameter-to-thickness ratios of 16.5, 31.0 and 60.0 were considered. The experimental results revealed that the moment-curvature relationship exhibited an almost steady loop from the beginning of the first cycle. Due to small and localized grooves, the groove depth showed almost no influence on the moment-curvature relationship for local sharp-grooved 6061-T6 aluminum alloy tubes with a certain diameter-to-thickness ratio. In contrast, the ovalization-curvature relationship depicted an increasing and ratcheting way along with the bending cycle, while the groove depth showed a strong influence on this relationship. In addition, the finite element software ANSYS was used to analyze the moment-curvature and ovalization-curvature relationships. Through comparison with the experimental data, the ANSYS could properly simulate the experimental findings. Because the failure type was the fatigue fracture, the ANSYS was used to calculate the maximum and minimum stresses and strains for each cyclic bending case. Finally, according to the distribution of stress or strain amplitudes and fatigue life on a log-log scale, relevant fatigue models were proposed.

Keywords: *Local Sharp-grooved 6061-T6 Aluminum Alloy Tubes, Different Diameter-to-thickness Ratios, Groove Depths, Cyclic Bending, Moment, Curvature, Ovalization, Finite Element ANSYS Analysis, Fatigue Life, Fatigue Models.*

1. Introduction

In 1998, Pan et al. [1] designed and set up a new measurement apparatus. The apparatus was used with a cyclic bending machine to study various types of tube under different cyclic bending conditions. For examples: Pan and Fan [2] studied the effect of the prior curvature rate at the preloading stage on subsequent creep or relaxation behavior, Pan and Her [3] investigated the response and stability of 304 stainless steel tubes that were subjected to cyclic bending with different curvature rate, Lee et al. [4] studied the influence of the diameter-to-thickness ratio on the response and collapse of circular tubes under symmetrical cyclic bending, Lee et al. [5] experimentally explored the effect of the diameter-to-thickness ratio and curvature rate on the response and stability of circular tubes subjected to cyclic bending, Chang et al. [6] studied the mean moment effect on circular, thin-walled tubes under cyclic bending, and Chang and Pan [7] discussed the buckling life estimation of circular tubes subjected to cyclic bending.

In 2010, the research team of Prof. Pan began to experimentally and analytically investigate the response and the collapse of sharp-notched circular tubes submitted to cyclic bending. Lee et al. [8] experimentally studied the relationship between the variation of ovalization and the number of bending cycles for sharp-notched circular tubes subjected to cyclic bending. They discovered that the aforementioned relationship could be clearly divided into three stages, namely initial, secondary, and tertiary. Lee [9] then later investigated the response of sharp-notched SUS304 stainless steel tubes under cyclic bending, and found the asymmetrical, ratcheting, and increasing trends of ovalization-curvature relationships. In addition, Lee et al. [10] evaluated the viscoplastic response and buckling of sharp-notched SUS304 stainless steel circular tubes undertaking cyclic bending. Both the different notch depths and curvature rates were examined. They observed that the controlled curvature-number of cycles required to ignite buckling relationships on a log-log scale revealed parallel lines for every notch depth for a certain curvature rate. Lee et al. [11] studied the response of sharp-notched SUS304 stainless steel tubes submitted to pure bending creep and pure bending relaxation. The Bailey-Norton law was modified for simulating the creep strain-time and relaxation stress-time relationships. Chung et al. [12] investigated the response and stability of sharp-notched 6061-T6 aluminum alloy tubes under cyclic bending. The controlled curvature-number of cycles required to ignite buckling relationship exhibited marked differences from the corresponding relationship observed in the cyclic-bended sharp-notched SUS304 stainless steel tubes tested by Lee et al. [10]. However, the sharp notch for the aforementioned studies was a circumferential sharp notch as shown in Fig. 1.

Fig. 1 A picture of the circumferential sharp-notched tube.

Later, Lee et al. [13] studied the response and failure life of 6061-T6 aluminum alloy tubes with a local sharp notch (Fig. 2) subjected to cyclic bending. In addition, the finite element software ANSYS was employed to analyze the moment-curvature and ovalization-curvature relationships. Lee et al. [14] investigated the response and stability of SUS304 stainless steel tubes with local sharp-notched (Fig. 3) depths of 0.2, 0.4, 0.6, 0.8, and 1.0 mm and notch directions of 0°, 30°, 60°, and 90° under cyclic bending. Finite element analysis via ANSYS was used to simulate the moment-curvature and ovalization-curvature relationships, and an empirical model was proposed to simulate the controlled curvature-number of cycles required to ignite buckling relationship.
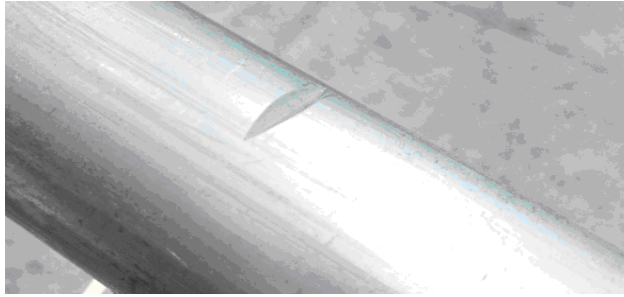

Fig. 2 A picture of the local sharp-notched (sharp-cut) tube.

Fig. 3 A picture of the local sharp-notched (sharp-grooved) tube.

In this study, local sharp-grooved 6061-T6 aluminum alloy tubes with different diameter-to-thickness ratios submitted to cyclic bending were experimentally investigated. The tube-bending machine and curvature-ovalization measurement apparatus were employed to conduct curvature-controlled cyclic bending tests. The quantities of moment, curvature and ovalization were measured by the testing devices. Additionally, the number of bending cycles required to ignite failure was also recorded.

2. Experiments

2.1 Experimental Devices

Fig. 4 schematically shows the experiment executed by a specially built tube-bending machine. This facility was set up to conduct monotonic, reverse, and cyclic bending tests. A detailed explanation of the experimental facility can be found in many papers (e.g., Pan and Her [3], Lee et al. [4]). Pan et al. [1] designed a new light-weight apparatus to measure the curvature and ovalization of the tube shown in Fig. 5. Two side-inclinometers in the apparatus were used to detect the angle variation of tubes during cyclic bending. The value of curvature can be obtained by a easy calculation according to angle changes.
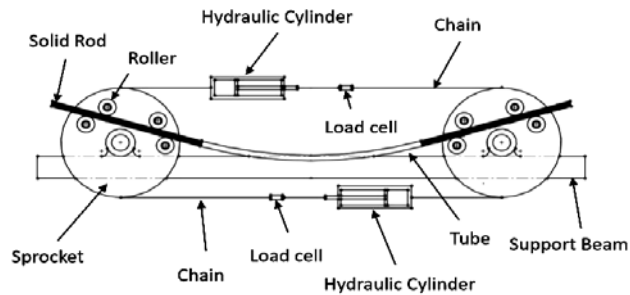
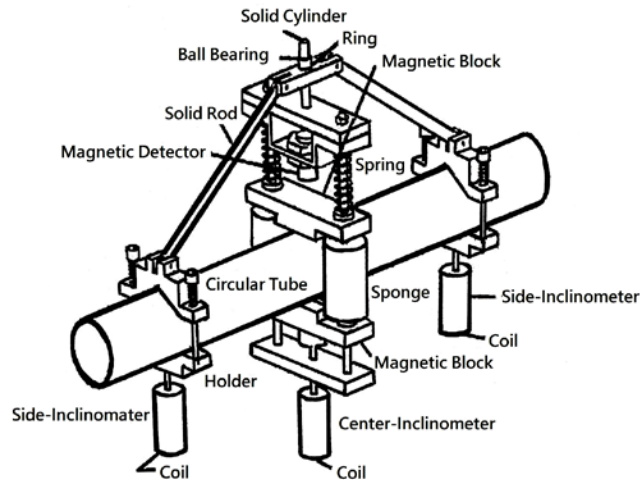Fig. 4 A schematic drawing of the tube-bending machine.

Fig. 5 A schematic drawing of the curvature-ovalization measurement apparatus.

2.2 Material and Specimens

6061-T6 aluminum alloy tubes were adopted for the cyclic bending tests. The tubes' chemical composition (weight %) is Mg (0.937), Si (0.535), Fe (0.139), Zn (0.098), Mn (0.022), Cr (0.022), …., and a few other trace elements, with the remainder being Al. The 0.2% strain offset yield stress is 285 MPa, the ultimate tensile stress is 320 MPa and the percent elongation is 23 %.

The raw, smooth 6061-T6 aluminum alloy circular tubes had a length L_o of 800 mm, a D_o of 35.0 mm and a t of 3.0 mm. The raw tubes were machined on the outside surface to obtain the desired D_o/t ratios of 16.5, 31.0 and 60.0 as shown in Fig. 6. Next, tubes with a certain D_o/t ratio were processed on the outside surface again to obtain the desired shape and depth of the groove. Fig. 7 shows a schematic drawing of the local sharp-grooved circular tube, where the groove depth is denoted as a. In this study, five different as were considered for each D_o/t. For tubes with $D_o/t = 16.5$, the values of a were 0.0, 0.3, 0.6, 0.9, and 1.2 mm. Based on the drill of the machine, the corresponding surface diameters (b) of tubes were 0.0, 0.9, 1.8, 2.7 and 3.6 mm, respectively. For tubes with $D_o/t = 31.0$, the values of a were 0.0, 0.15, 0.3, 0.45, and 0.6 mm. The corresponding b were 0.0, 0.45, 0.9, 1.35 and 1.8 mm, respectively. For tubes with $D_o/t = 60.0$, the values of a were 0.0, 0.08, 0.15, 0.23, and 0.3 mm. The corresponding b were 0.0, 0.24, 0.45, 0.69 and 0.9 mm,

respectively. Note that $a = 0.0$ mm represents a tube with a smooth surface. Fig. 8 shows a picture of local sharp-grooved 6061-T6 aluminum alloy tubes with $D_o/t = 16.5$ and $a = 0.0, 0.3, 0.6, 0.9$ and 1.2 mm.
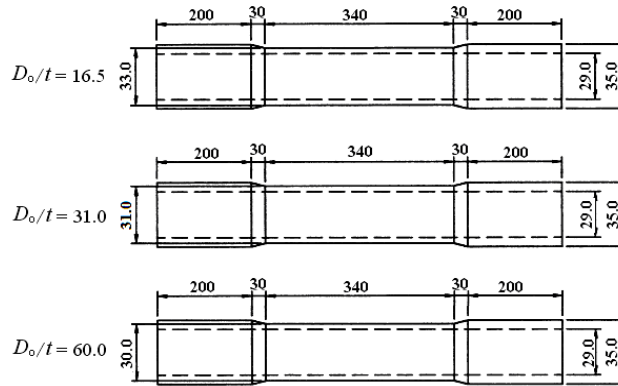

Fig. 6 A schematic drawing of tube's dimensions for D_o/t ratios of 16.5, 31.0 and 60.0.

2.3 Test Procedures

The test involved a curvature-controlled cyclic bending. The controlled-curvature ranges were from ± 0.2 to ± 1.3 m^{-1}, and the curvature rate of the cyclic bending test was 0.035 m^{-1}s^{-1}. The magnitude of the moment was measured by two load cells mounted to the bending device. The magnitude of the curvature and ovalization were controlled and measured by the curvature-ovalization measurement apparatus. In addition, the the number of bending cycles required to ignite failure was also recorded.
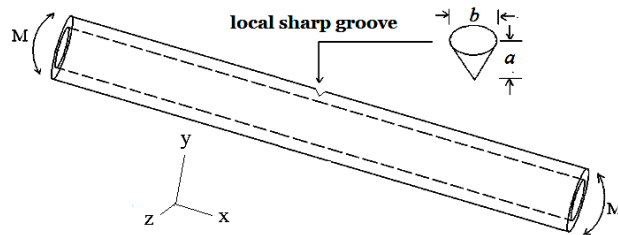

Fig. 7 A schematic drawing of the local sharp-grooved circular tube.

Fig. 8 A picture of local sharp-grooved 6061-T6 aluminum alloy tubes with $D_o/t = 16.5$ and $a = 0.0, 0.3, 0.6, 0.9$ and 1.2 mm.

3. Finite Element ANSYS Analysis

The mechanical behavior of local sharp-grooved circular tubes subjected to cyclic bending was numerically analyzed using the finite element software ANSYS. The mechanical behavior of tubes presented the relationship between moment and curvature, as well as that between ovalization and curvature. The elastic-plastic stress-strain response, model, mesh, boundary conditions, and loading conditions are introduced in next sections.

3.1 Elastic-plastic Stress-strain Curves

Fig. 9 shows the tested and ANSYS- constructed uniaxial stress (σ)-strain (ε) curves of the 6061-T6 aluminum alloy steel. The kinematic hardening rule was used as the hardening rule for reverse and cyclic loading.

3.2 ANSYS Element and Model

Owing to the three-dimensional geometry and elastic-plastic deformation of the tube, the SOLID 185 element was used for relative analysis. This element is a tetrahedral element built in ANSYS that is suitable for analyzing plastic and large deformations. In particular, this element is adequate for analyzing shell components subjected to bending. Owing to the right-left symmetry of tubes, only half of the tube model was constructed. Fig. 10 shows the mesh constructed by ANSYS.
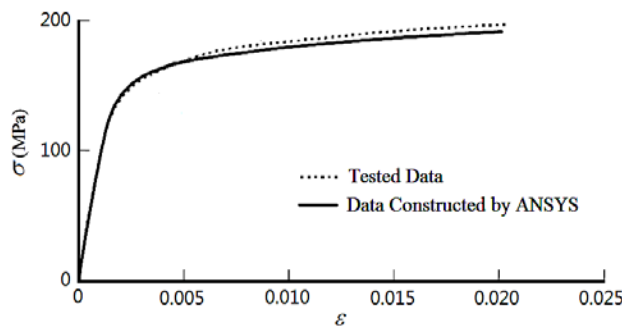

Fig. 9 Tested and ANSYS-constructed data of the uniaxial σ-ε curve for 6061-T6 aluminum alloy.
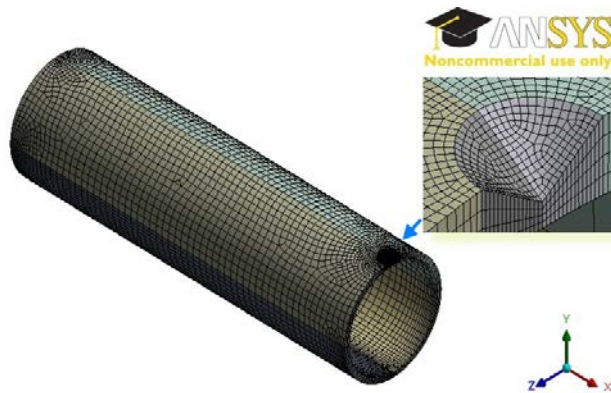

Fig. 10 Mesh constructed by ANSYS for half tube.

3.3 Boundary and Loading Conditions

Fig. 11 shows the restrictions on the symmetrical plane (central cross-section), as constructed by ANSYS, for a tube subjected to cyclic bending. Since the tubes were bent in the z-direction only, the frictionless roller support was fixed to the symmetrical plane and the displacement in the z-direction of this plane was set to zero. Fig. 12 shows the loading conditions constructed by ANSYS on the basis of the tube-bending device; here, the remote displacement in the z-direction was unrestricted, i.e., the rotation was free to move in the z-direction. In addition, the bending moment was applied only in the z-direction; hence, the rotations in the x- and y-directions were set to zero.

Fig. 13 demonstrates a tube subjected to pure bending. The rotation angle θ for the curvature-controlled cyclic bending was used as the input data, and curvature (κ) was related to θ as follows:

$$\kappa = 1 \, / \, \rho = 2\theta \, / \, L_{o,} \qquad\qquad (1)$$

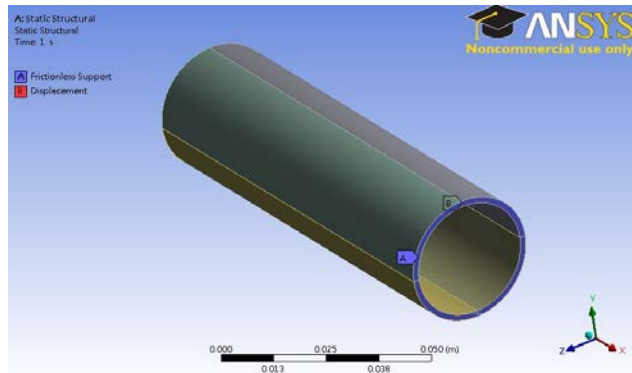where ρ is the radius of the curvature, and L_o is the original tube length.

Fig. 11 Restrictions on the symmetrical plane constructed by ANSYS.
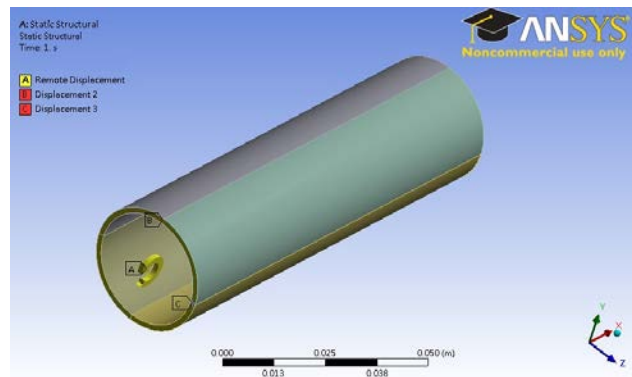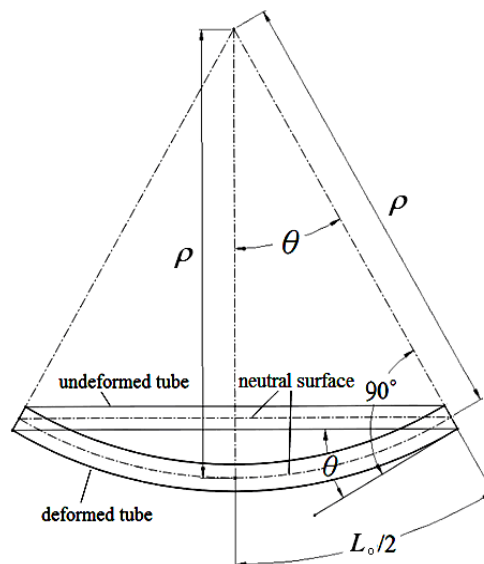

Fig. 12 Loading condition constructed by ANSYS.

Fig. 13 Relationship between θ and κ for a tube under pure bending.

4. Experimental and Simulated Results

4.1 Mechanical Response

Figs. 14(a)-(c) shows typical sets of experimentally determined cyclic moment (M)-curvature (κ) curves for local sharp-grooved 6061-T6 aluminum alloy circular tubes with a = 0.3 mm and D_o/t = 16.5, 31.0 and 60.0, respectively, subjected to cyclic bending. The tubes were cycled between κ = ±0.4 m^{-1}. It was observed that the M-κ relationship was seen to be characterized by a nearly closed and steady hysteresis loop from the first bending cycle. Since the sharp groove is small and local, the groove depth has almost no influence on the M-κ curve. Therefore, the M-κ curves for different as and D_o/t ratios are not shown in this paper. Figs. 15(a)-(c) show the M-κ curves of Figs. 14(a)-(c) as simulated by ANSYS.
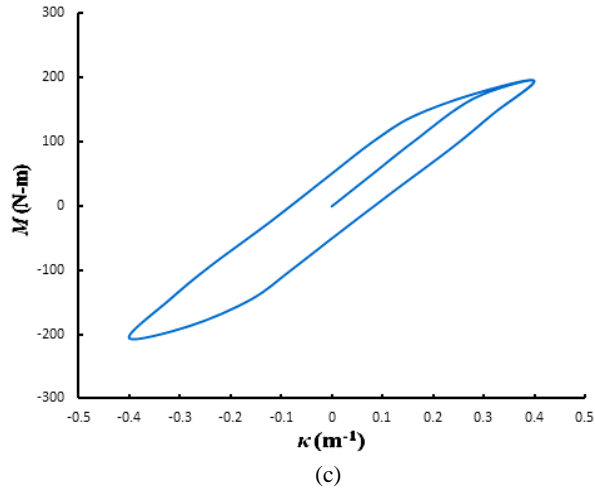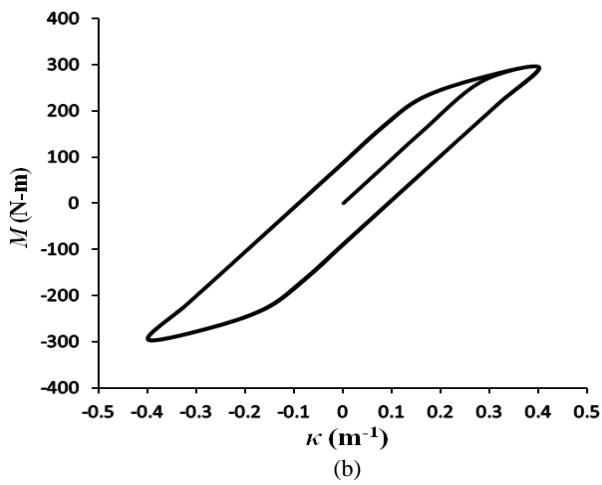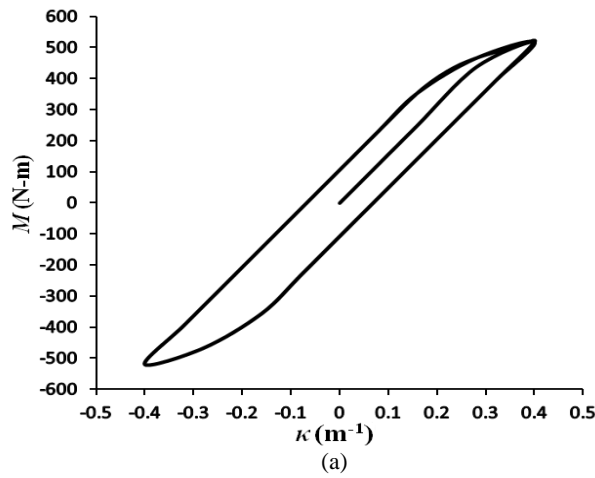

(a)

(b)

(c)
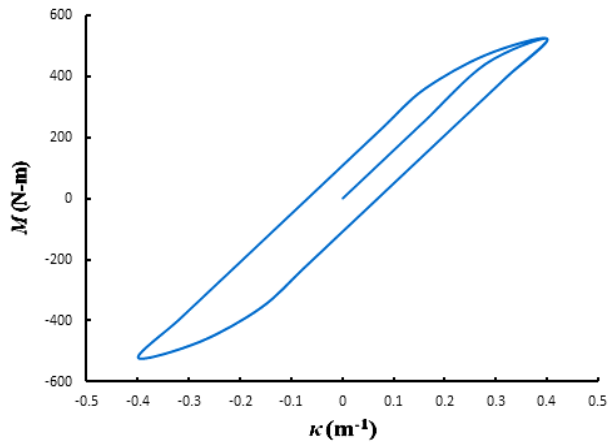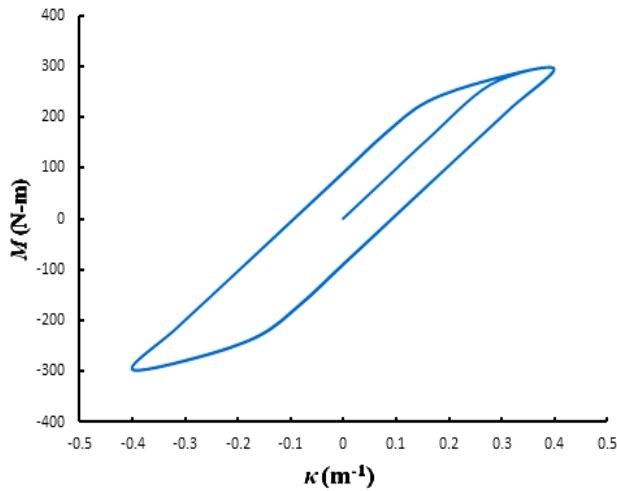
Fig. 14 Experimental M-κ curves for local sharp-grooved 6061-T6 aluminum alloy tubes with $a = 0.3$ mm and $D_o/t =$ (a) 16.5, (b) 31.0 and (c) 60.0 under cyclic bending.

(a)

(b)

(c)

Fig. 15 ANSYS-simulated M-κ curves for local sharp-grooved 6061-T6 aluminum alloy tubes with a = 0.3 mm and D_o/t = (a) 16.5, (b) 31.0 and (c) 60.0 under cyclic bending.
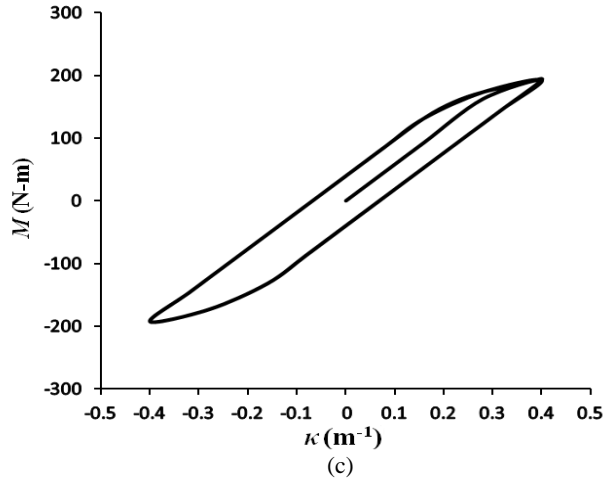
Figs. 16(a)-(e) depict the experimental ovalization ($\Delta D_o/D_o$)-curvature (κ) curves for local sharp-grooved 6061-T6 aluminum alloy tubes with D_o/t = 16.5 and a = 0.0, 0.3, 0.6, 0.9, and 1.2 mm, respectively, subjected to cyclic bending. The tubes were also cycled between κ = ±0.4 m^{-1}. The $\Delta D_o/D_o$-κ relationships exhibited a ratcheting and an increasing trend with the number of bending cycles. A larger a led to a more asymmetrical appearance of the $\Delta D_o/D_o$-κ relationship. Moreover, a larger a of the sharp-grooved tubes caused a larger ovalization. Figs. 17(a)-(e) demonstrate the ANSYS-simulated $\Delta D_o/D_o$-κ curves for local sharp-grooved 6061- T6 aluminum alloy tubes with D_o/t = 16.5 and a = 0.0, 0.3, 0.6, 0.9, and 1.2 mm, respectively, under cyclic bending.
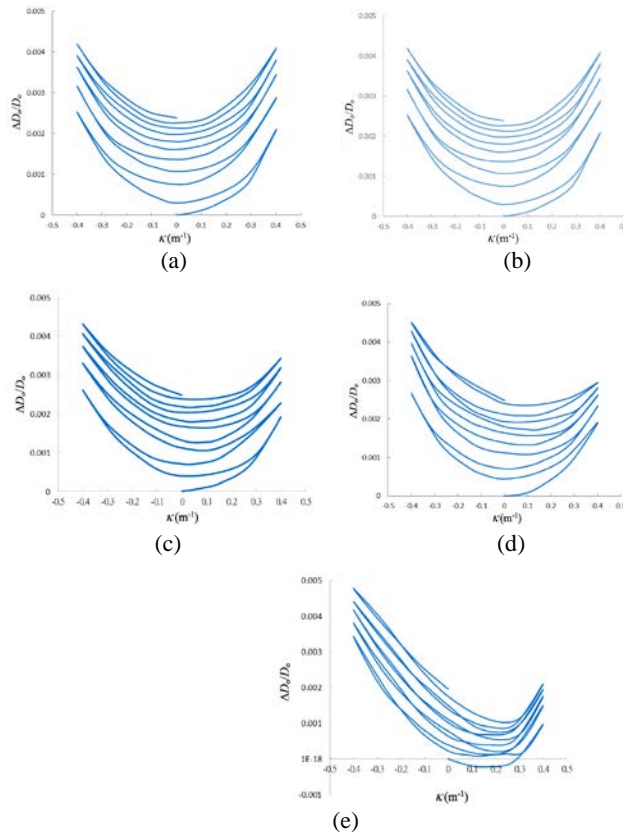

(a)

(b)

(c)

(d)

(e)

Fig. 16 Experimental $\Delta D_o/D_o$-κ curves for local sharp-grooved 6061-T6 aluminum alloy tubes with $D_o/t = 16.5$ and $a =$ (a) 0.0, (b) 0.3, (c) 0.6, (d) 0.9 and (e) 1.2 mm under cyclic bending.

(a)

(b)

(c)

(d)

(e)

Fig. 17 ANSYS-simulated $\Delta D_o/D_o$-κ curves for local sharp-grooved 6061-T6 aluminum alloy tubes with $D_o/t = 16.5$ and $a =$ (a) 0.0, (b) 0.3, (c) 0.6, (d) 0.9 and (e) 1.2 mm under cyclic bending.
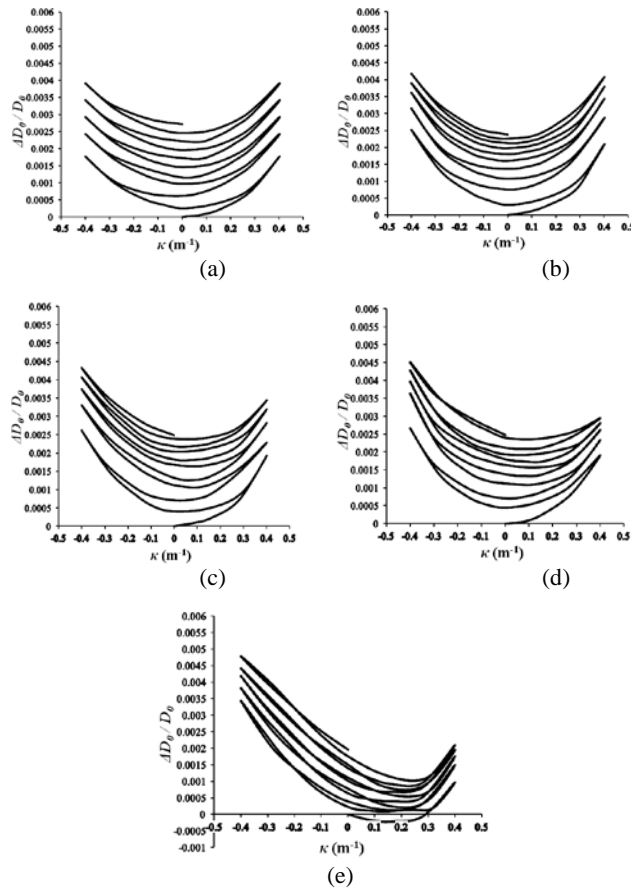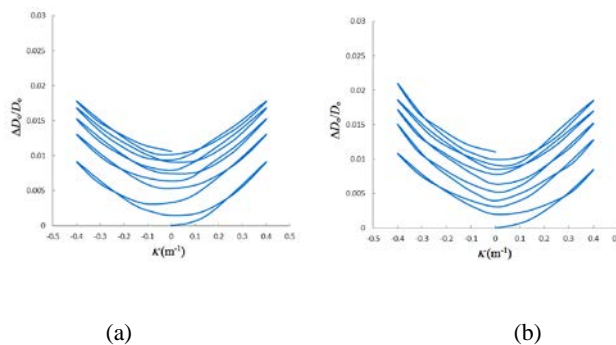
Figs. 18(a)-(e) depict the experimental $\Delta D_o/D_o$-κ curves for local sharp-grooved 6061-T6 aluminum alloy tubes with $D_o/t = 31.0$ and $a = 0.0, 0.15, 0.3, 0.45,$ and 0.6 mm respectively, subjected to cyclic bending. Figs. 20(a)-(e) show the experimental $\Delta D_o/D_o$-κ curves for local sharp- grooved 6061-T6 aluminum alloy tubes with $D_o/t = 60.0$ and $a = 0.0, 0.08, 0.15, 0.23,$ and 0.3 mm, respectively, under cyclic bending. Similar phenomena with local sharp-grooved 6061-T6 aluminum alloy tubes with $D_o/t = 16.5$ were found. In addition, a larger D_o/t ratio has a smaller t, thus, the $\Delta D_o/D_o$ increases faster. Figs. 19(a)-(e) depict the ANSYS-simulated $\Delta D_o/D_o$-κ curves for local sharp-grooved 6061-T6 aluminum alloy tubes with $D_o/t = 31.0$ and $a = 0.0, 0.15, 0.3, 0.45,$ and 0.6 mm respectively, under cyclic bending. Figs. 21(a)-(e) show the ANSYS-simulated $\Delta D_o/D_o$-κ curves for local sharp-grooved 6061-T6 aluminum alloy tubes with $D_o/t = 60.0$ and $a = 0.0, 0.08, 0.15, 0.23,$ and 0.3 mm, respectively, subjected to cyclic bending.

(a)

(b)

Fig. 18 Experimental $\Delta D_o/D_o$-κ curves for local sharp-grooved 6061-T6 aluminum alloy tubes with $D_o/t = 31.0$ and $a =$ (a) 0.0, (b) 0.15, (c) 0.3, (d) 0.45 and (e) 0.6 mm under cyclic bending.

Fig. 19 ANSYS-simulated $\Delta D_o/D_o$-κ curves for local sharp-grooved 6061-T6 aluminum alloy tubes with $D_o/t = 31.0$ and $a =$ (a) 0.0, (b) 0.15, (c) 0.3, (d) 0.45 and (e) 0.6 mm under cyclic bending.

Fig. 20 Experimental $\Delta D_{o}/D_{o}$-κ curves for local sharp-grooved 6061-T6 aluminum alloy tubes with $D_{o}/t = 60.0$ and $a =$ (a) 0.0, (b) 0.08, (c) 0.15, (d) 0.23 and (e) 0.3 mm under cyclic bending.

(e)

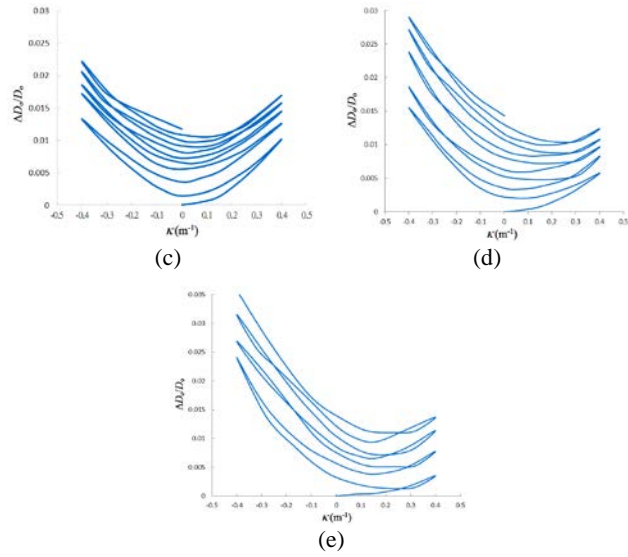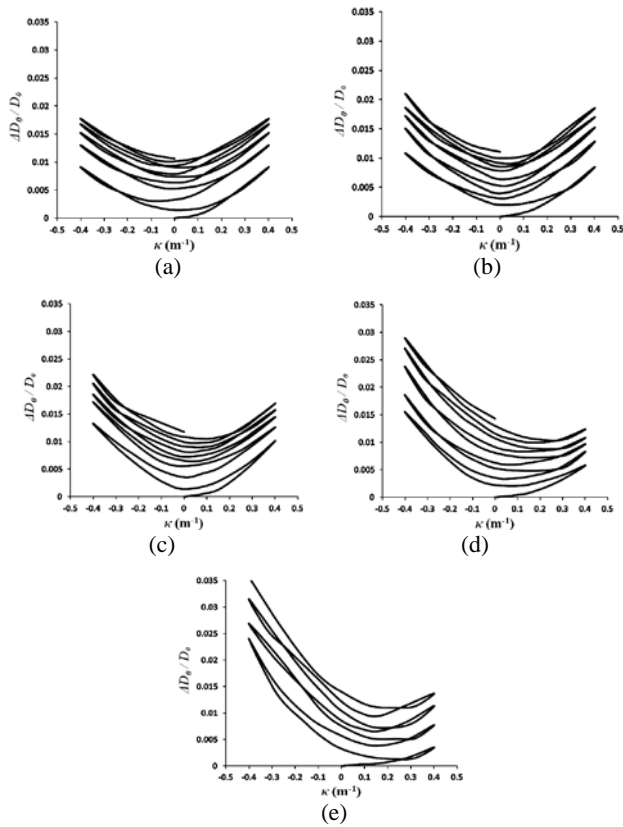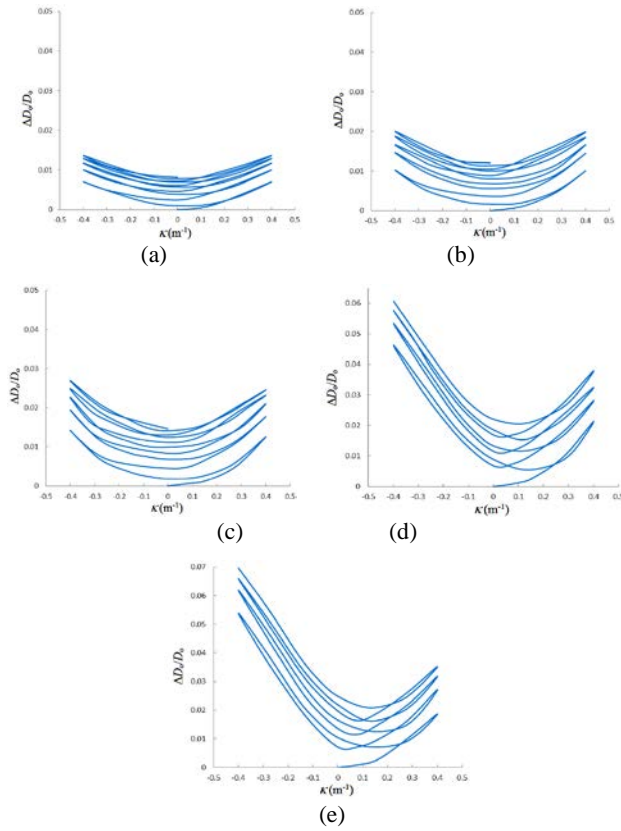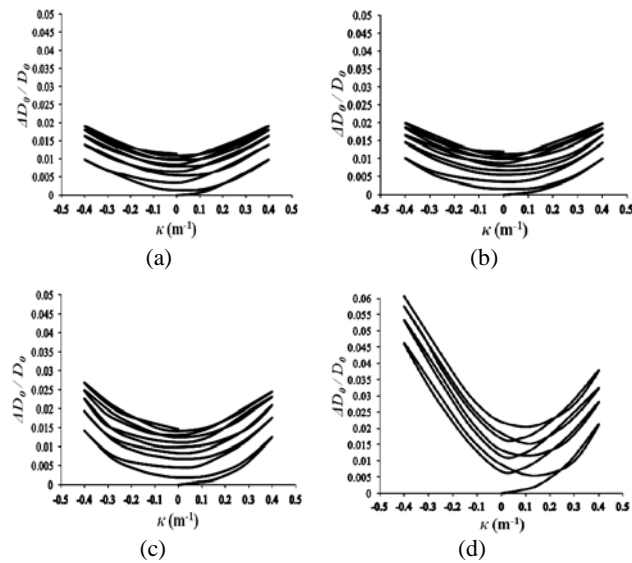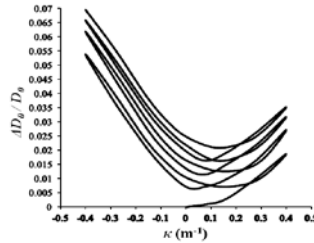Fig. 21 ANSYS-simulated $\Delta D_o/D_o$-κ curves for local sharp-grooved 6061-T6 aluminum alloy tubes with $D_o/t = 60.0$ and $a = $ (a) 0.0, (b) 0.08, (c) 0.15, (d) 0.23 and (e) 0.3 mm under cyclic bending.

4.2 Fatigue Failure

We discovered that the failure type of local sharp-grooved 6061-T6 aluminum alloy tubes under cyclic bending was the fatigue fracture. Because the finite element ANSYS could accurately simulate the M-κ and $\Delta D_o/D_o$-κ relationships (Figs. 15(a)-(c), Figs. 17(a)-(e), Figs. 19(a)-(e) and Figs. 21(a)-(e)), so the ANSYS was used to calculate the maximum stress (σ_{max}), minimum stress (σ_{min}), maximum strain (ε_{max}) and minimum strain (ε_{min}) for each cyclic bending case. Figs. 22(a)-(b) respectively show the stress and strain distribution of local sharp-grooved 6061-T6 aluminum alloy tubes with D_o/t =16.5 and a = 0.3 mm. The κ is +0.32 m^{-1}. The σ_{max} and ε_{max} are 94.777 MPa and 0.0024548 at the groove, respectively.

Tables 1 show the σ_{max} and σ_{min} for local sharp-grooved 6061-T6 aluminum alloy circular tubes with D_o/t =16.5 subjected to cyclic bending and Tables 2 show the ε_{max} and ε_{min} for local sharp-grooved 6061-T6 aluminum alloy circular tubes with D_o/t =16.5 subjected to cyclic bending. The amount of a and κ are also demonstrated in these tables. The magnitudes of stress and strain were determined by ANSYS discussed in Sec. 3. Due to the symmetrical curvature-controlled cyclic bending (the maximum control curvature equals to the minimum control curvature) and a local and small groove, the amounts of maximum and minimum stresses and strains were not much difference for each loading case. Therefore, the mean stress effect did not consider in the fatigue analysis.
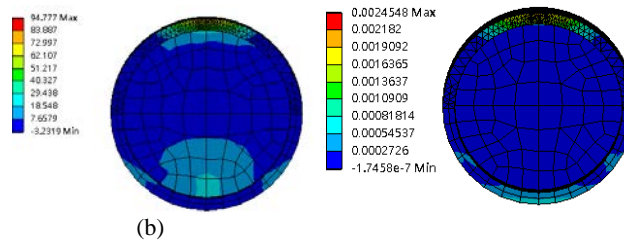
(a)   (b)

Fig. 22 The (a) stress and (b) strain distribution of local sharp-grooved 6061-T6 aluminum alloy tubes with D_o/t =16.5, a = 0.3 mm and κ = +0.3 m^{-1}.

Table 1 σ_{max} and σ_{min} for local sharp-grooved 6061-T6 aluminum alloy circular tubes with D_o/t =16.5 under cyclic bending.

a (mm)	κ (m^{-1})	σ_{max} (MPa)	σ_{min} (MPa)
0	0.23	55.359	-69.044
0	0.24	71.821	-87.781
0	0.30	81.641	-97.789
0	0.31	90.997	-106.820
0	0.34	108.839	-125.221
0	0.42	120.964	-136.412
0	0.57	195.153	-215.722
0	0.67	211.504	-224.130
0.3	0.23	64.084	-86.702
0.3	0.27	80.758	-102.781
0.3	0.32	94.777	-114.259

0.3	0.35	158.452	-178.681
0.3	0.40	173.852	-182.130
0.3	0.55	215.221	-220.171
0.3	0.68	237.123	-245.042
0.6	0.30	104.563	-120.461
0.6	0.33	132.436	-158.560
0.6	0.39	164.601	-185.612
0.6	0.42	191.631	-207.043
0.6	0.46	208.853	-215.844
0.6	0.70	237.416	-250.211
0.9	0.34	162.752	-185.540
0.9	0.39	207.422	-224.023
0.9	0.47	212.538	-219.191
0.9	0.61	244.676	-248.697
1.2	0.30	157.079	-171.796
1.2	0.33	209.045	-212.484
1.2	0.35	220.478	-226.621
1.2	0.42	235.916	-238.483
1.2	0.50	244.522	-247.145

Table 2 ε_{max} and ε_{min} for local sharp-grooved 6061-T6 aluminum alloy circular tubes with D_o/t =16.5 under cyclic bending.

a (mm)	κ (m^{-1})	ε_{max} ($\times 10^{-3}$)	ε_{min} ($\times 10^{-3}$)
0	0.23	1.0849	-1.3531
0	0.24	1.5999	-1.9554
0	0.30	1.7219	-2.0626
0	0.31	2.1801	-2.5593
0	0.34	2.5308	-2.9118
0	0.42	2.9602	-3.3382
0	0.57	4.0092	-4.4312
0	0.67	4.3531	-4.7159
0.3	0.23	1.6576	-2.2427
0.3	0.27	2.0593	-2.6210
0.3	0.32	2.4548	-2.9879
0.3	0.35	2.6927	-3.0364
0.3	0.40	3.0022	-3.1879
0.3	0.55	4.9137	-5.0124
0.3	0.68	5.6577	-5.8687
0.6	0.30	2.4256	-2.9150
0.6	0.33	2.7648	-3.2643
0.6	0.39	3.1437	-3.5451
0.6	0.42	4.1363	-4.2505
0.6	0.46	4.4172	-4.6312
0.6	0.70	6.3212	-6.4066
0.9	0.34	2.9705	-3.9377
0.9	0.39	4.1339	-4.8529
0.9	0.47	5.7418	-6.1843
0.9	0.61	8.2184	-8.5094
1.2	0.30	3.2608	-3.8280
1.2	0.33	4.5995	-4.7873
1.2	0.35	4.7899	-4.9984
1.2	0.42	6.4693	-6.7568
1.2	0.50	8.5584	-8.8457

Fig. 23 shows the experimental data of the stress amplitude (σ_a) versus $2N_f$ in solid black circles for local sharp-grooved 6061-T6 aluminum alloy circular tubes with different D_o/t ratios subjected to cyclic bending on a log-log scale. Note that $\sigma_a = (\sigma_{max} - \sigma_{min}) / 2$. It was observed that although all data can be considered to be in a straight line, all the data seems to be a bit scattered.

A simple fatigue model was proposed to be

$$\sigma_a = \sigma_f^{'} (2N_f)^b \qquad (2)$$

or

$$\log \sigma_a = \log \sigma_f^{'} + b \log(2N_f) \qquad (3)$$

where $\sigma_f^{'}$ and b are the fatigue strength coefficient and fatigue strength exponent, respectively. The straight line in Fig. 23 was determined by least-square fit. The magnitudes of $\sigma_f^{'}$ and b were determined to be 294.118 MPa and -0.2167, respectively.
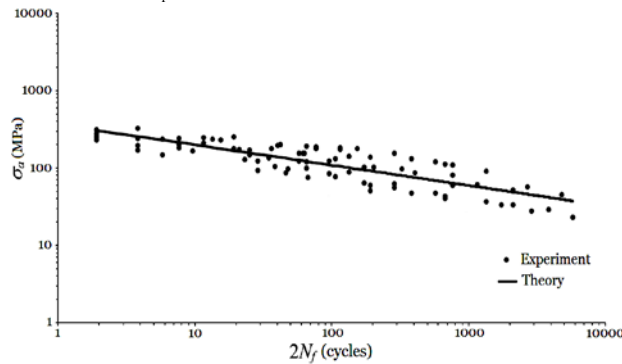

Fig. 23 Experimental and simulated σ_a-$2N_f$ relationships for local sharp-grooved 6061-T6 aluminum alloy circular tubes with different D_o/t ratios under cyclic bending on a log-log scale.

Fig. 24 shows the experimental data of the strain amplitude (ε_a) versus $2N_f$ in solid black circles for local sharp-grooved 6061-T6 aluminum alloy circular tubes with different D_o/t ratios subjected to cyclic bending on a log- log scale. Note that $\varepsilon_a = (\varepsilon_{max} - \varepsilon_{min}) / 2$. It can be seen in Fig. 24 that the experimental ε_a-N_f data were almost in a straight line. Therefore, a simple fatigue model was proposed to be

$$\varepsilon_a = \varepsilon_f^{'} (2N_f)^c \qquad (4)$$

or

$$\log \varepsilon_a = \log \varepsilon_f^{'} + c \log(2N_f) \qquad (5)$$

where $\varepsilon_f^{'}$ and c are the fatigue ductility coefficient and fatigue ductility exponent, respectively. The straight line in Fig. 24 was determined by least-square fit. The magnitudes of $\varepsilon_f^{'}$ and c were determined to be 0.01407 and -0.2576, respectively.
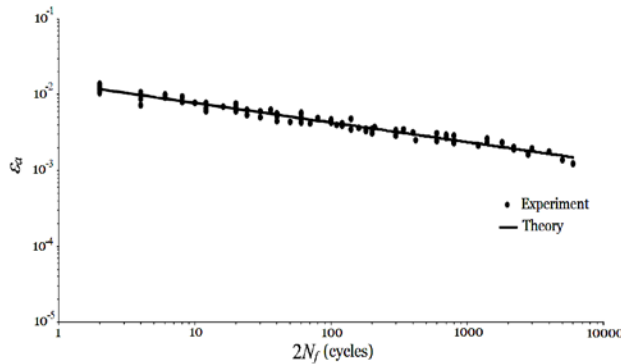

Fig. 24 Experimental and simulated ε_a-$2N_f$ relationships for local sharp-grooved 6061-T6 aluminum alloy circular tubes with different D_o/t ratios under cyclic bending on a log-log scale.

5. Conclusions

This study investigated the response and failure of the local sharp-grooved 6061-T6 aluminum alloy tubes with different D_o/t ratios submitted to cyclic bending. Some important conclusions are sorted as follows according to the experimental and simulated results:

(1) The experimental M-κ relationship for local sharp-grooved 6061-T6 aluminum alloy tubes with any a or D_o/t ratio displayed a closed hysteresis loop from the first bending cycle. Since the sharp groove was small and local, the a had almost no influence on the M-κ curve for a certain D_o/t ratio.

(2) The experimental $\Delta D_o/D_o$-κ relationship for local sharp-grooved 6061-T6 aluminum alloy tubes with any D_o/t ratio or a revealed an increasing and ratcheting trend with the number of bending cycles. In addition, the tubes with a larger D_o/t or a led to more asymmetrical trend and a larger ovalization.

(3) Using adequate stress-strain curve, mesh, boundary conditions and loading conditions, the finite element software ANSYS was used for simulating the behavior of local sharp-grooved circular tubes under cyclic bending; this behavior included the M-κ and $\Delta D_o/D_o$-κ relationships. The simulated results exhibited close correspondence to those obtained from experiments.

(4) According to the ε_a-$2N_f$ relationship for local sharp-grooved 6061-T6 aluminum alloy circular tubes with different D_o/t ratios under cyclic bending. A simple fatigue model (Eq. (4)) was proposed and parameters ε_f' and c were determined to be 0.01407 and -0.2576, respectively. It was found that the simulation was in good agreement with the experimental result as shown in Fig. 24.

Acknowledgment

References

[1] W. F. Pan, T. R. Wang and C. M. Hsu, "A curvature-ovalization measurement apparatus for circular tubes under cyclic bending," Exp. Mech., Vol. 38, No. 2, 1998, pp. 99-102.

[2] W. F. Pan and C. H. Fan, "An experimental study on the effect of curvature-rate at preloading stage on subsequent creep or relaxation of thin-walled tubes under pure bending," JSME Int. J., Ser. A, Vol. 41, No. 4, 1998, pp. 525-531.

[3] W. F. Pan and Y. S. Her, "Viscoplastic collapse of thin-walled tubes under cyclic bending," J. Eng. Mat. Tech., Vol. 120, No. 4, 1998, pp. 287-290.

[4] K. L. Lee, W. F. Pan and J. N. Kuo, "The influence of the diameter-to-thickness ratio on the stability of circular tubes under cyclic bending," Int. J. Solids Struct., Vol. 38, No. 14, 2001, pp. 2401-2413.

[5] K. L. Lee, W. F. Pan and C. M. Hsu, "Experimental and theoretical evaluations of the effect between diameter-to- thickness ratio and curvature-rate on the stability of circular tubes under cyclic bending," JSME Int. J., Ser. A, Vol. 47, No. 2, 2004, pp. 212-222.

[6] K. H. Chang and W. F. Pan and K. L. Lee, "Mean moment effect of thin-walled tubes under cyclic bending," Struct. Eng. Mech., Vol. 28, No. 5, 2008, pp. 495-514.

[7] K. H. Chang and W. F. Pan, "Buckling life estimation of circular tubes under cyclic bending," Int. J. Solids Struct., Vol. 46, No. 2, 2009, pp. 254-270.

[8] K. L. Lee, C. Y. Hung and W. F. Pan, "Variation of ovalization for sharp-notched circular tubes under cyclic bending," J. Mech., Vol. 26, No. 3, 2010, pp. 403- 411.

[9] K. L. Lee, "Mechanical behavior and buckling failure of sharp-notched circular tubes under cyclic bending," Struct. Eng. Mech., Vol. 34, No. 3, 2010, pp. 367-376.

[10] K. L. Lee, C. M. Hsu and W. F. Pan, "Viscoplastic collapse of sharp-notched circular tubes under cyclic bending," Acta Mech. Solida Sinica, Vol. 26, No. 6, 2013, pp. 629-641.

[11] K. L. Lee, C. M. Hsu and W. F. Pan, "Response of sharp-notched circular tubes under bending creep and relaxation," Mech. Eng. J., Vol. 1, No. 2, 2014, pp. 1-14.

[12] C. C. Chung, K. L. Lee and W. F. Pan, "Collapse of sharp-notched 6061-T6 aluminum alloy tubes under cyclic bending," Int. J. Struct. Stab. Dyn., Vol. 26, No. 7, 2016, 1550035 [24 pages].

[13] K. L. Lee, K. H. Chang and W. F. Pan, "Failure life estimation of sharp-notched circular tubes with different notch depths under cyclic bending," Struct. Eng. Mech., Vol. 60, No. 3, 2016, pp. 387-404.

[14] K. L. Lee, K. H. Chang and W. F. Pan, "Effects of notch depth and direction on stability of local sharp-notched circular tubes subjected to cyclic bending," Int. J. Struct. Stab. Dyn., Vol. 18, No. 7, 2018, 1850099 [23 pages].

Kuo-Long Lee received the Ph.D. degree in Dept. of Engineering Science from National Cheng Kung University in Taiwan in 2000. Currently working as Prof. in Dept. of Innovative Design and Entrepreneurship from Far East University in Taiwan.

Wen-Fung Pan received the Ph.D. degree in Dept. of Civil and Environmental Engineering from University of Iowa in USA in 1989. Currently working as Prof. in Dept. of Engineering Science from National Cheng Kung University in Taiwan.